Rescue of a Mouse Model of Spinal Muscular Atrophy With Respiratory Distress Type 1 by AAV9-IGHMBP2 Is Dose Dependent

Monir Shababi[1,2], Zhihua Feng[3], Eric Villalon[2,4], Christine M Sibigtroth[2,4], Erkan Y Osman[1,2], Madeline R Miller[2,5], Patricka A Williams-Simon[2,4], Abby Lombardi[2,4], Thalia H Sass[2,4], Arleigh K Atkinson[2,4], Michael L Garcia[2,4], Chien-Ping Ko[3] and Christian L Lorson[1,2,6]

[1]Department of Veterinary Pathobiology, College of Veterinary Medicine, University of Missouri, Columbia, Missouri, USA; [2]Bond Life Sciences Center, University of Missouri, Columbia, Missouri, USA; [3]Section of Neurobiology, Department of Biological Sciences, University of Southern California, Los Angeles, California, USA; [4]Department of Biological Sciences, College of Art and Sciences, University of Missouri, Columbia, Missouri, USA; [5]Genetics Area Program, Christopher S. Bond Life Sciences Center, University of Missouri, Columbia, Missouri, USA; [6]Department of Molecular Microbiology and Immunology, School of Medicine, University of Missouri, Columbia, Missouri, USA

Spinal muscular atrophy with respiratory distress type 1 (SMARD1) is an autosomal recessive disease occurring during childhood. The gene responsible for disease development is a ubiquitously expressed protein, IGHMBP2. Mutations in IGHMBP2 result in the loss of α-motor neurons leading to muscle atrophy in the distal limbs accompanied by respiratory complications. Although genetically and clinically distinct, proximal SMA is also caused by the loss of a ubiquitously expressed gene (SMN). Significant preclinical success has been achieved in proximal SMA using viral-based gene replacement strategies. We leveraged the technologies employed in SMA to demonstrate gene replacement efficacy in an SMARD1 animal model. Intracerebroventricular (ICV) injection of single-stranded AAV9 expressing the full-length cDNA of IGHMBP2 in a low dose led to a significant level of rescue in treated SMARD1 animals. Consistent with drastically increased survival, weight gain, and strength, the rescued animals demonstrated a significant improvement in muscle, NMJ, motor neurons, and axonal pathology. In addition, increased levels of IGHMBP2 in lumbar motor neurons verified the efficacy of the virus to transduce the target tissues. Our results indicate that AAV9-based gene replacement is a viable strategy for SMARD1, although dosing effects and potential negative impacts of high dose and ICV injection should be thoroughly investigated.

Received 31 August 2015; accepted 17 January 2016; advance online publication 8 March 2016. doi:10.1038/mt.2016.33

INTRODUCTION

Spinal muscular atrophy with respiratory distress type 1 (SMARD1) is an autosomal recessive motor neuron disease which affects children at infancy. SMARD1 is distinguished from 5q-linked SMA by the genetic mutation and the pathology. Unlike SMA in which muscle atrophy occurs in proximal muscle group, SMARD1 is initially characterized by distal lower limb muscle atrophy followed by proximal muscle weakness.[1,2] Respiratory complications in SMA arise from intercostal muscle atrophy while respiratory failure in SMARD1 is due to diaphragmatic paralysis which is the first major clinical symptom, typically manifesting between 6 weeks and 6–13 months of age.[1,3,4] Children with SMARD1 are usually completely paralyzed and require continuous artificial ventilation. In contrast to SMA, patients with SMARD1 display myelination changes in the peripheral nervous system.[5,6] SMARD1 patients show reduced diameter of myofibrils in skeletal muscle and a variety of muscle fiber diameters in the diaphragm.[7]

SMARD1 is caused by mutations in the *immunoglobulin μ-binding protein 2* (*IGHMBP2*) gene located on chromosome 11q13.3.[3,8,9] *IGHMBP2* is highly homologous to the mouse *IGHMBP2* gene, and a previously characterized mutation in this gene is responsible for the neurodegenerative *nmd* mouse model.[10] The *IGHMBP2* gene is ubiquitously expressed and comprises 15 exons encoding 993 amino acids corresponding to a ~110 kDa product. The exact disease-associated role of IGHMBP2 is unknown; however, the protein contains an ATP binding motif, a helicase-like motif, and two nucleic acid binding motifs. The gene product purportedly functions in immunoglobulin-class switching,[9] pre-mRNA maturation,[11] and transcription regulation by either DNA binding activity[12,13] or interaction with TATA-binding protein.[14] The direct interaction with tRNA and other components of translational machinery suggests that IGHMBP2 is also involved in translation.[15,16] The SMARD1 mouse model (*nmd*) contains a mutation in *IGHMBP2* intron 4, resulting in the creation of a cryptic splice site that disrupts the normal splicing ratio of IGHMBP2 transcripts.[10,17] This mutation leads to aberrant splicing in ~75–80% of the IGHMBP2 mRNAs producing merely 20–25% functional IGHMBP2 protein.[18] The protein product of abnormally spliced

The first author and the last author are the equally contributing senior authors.

Correspondence: *Christian L. Lorson, Department of Veterinary Pathobiology and Department of Molecular Microbiology and Immunology, University of Missouri, Bond Life Sciences Center, Columbia, Missouri 65211, USA. E-mail: lorsonc@missouri.edu*

mRNA is approximately 21 KDa and contains a truncated C terminus.[18] The most obvious physical characteristic of *nmd* mice is weakness and retrenchment in their hind limb when suspended from the tail that appears within second week of age,[18] consistent with a well-described hind limb muscle weakness that proceeds to the forelimb and trunk muscles. Cardiomyopathy is also observed in *nmd* mice but is very rare in SMARD1 patients. The life span of *nmd* mice is highly variable ranging from 10 weeks up to 7 months.[10,19]

Currently, there is no cure or effective therapy for SMARD1. With the recent advancements in vector-based gene therapy for CNS diseases such as SMA, there is considerable momentum in gene therapy for rare disorders. To evaluate the viability of gene replacement therapy in SMARD1, we administered an AAV9-IGHMBP2 vector to *nmd* mice and examined: (i) dosing effects; (ii) an intracerebroventricular (ICV) delivery; and (iii) the phenotypic rescue at functional and cellular levels. Our results suggest that the gene replacement therapy using a low dose greatly reduces the devastating effects of SMARD1 disease but also implies the potential negative impact of high dosage of the virus as well as ICV injection in *nmd* genetic background.

RESULTS

In vivo expression of AAV9-IGHMBP2

Self-complementary AAV (scAAV) provides rapid and robust transgene expression and has been utilized in several disease models, including SMA. Due to packaging limitation of scAAV9, we utilized single-stranded AAV9 to generate the AAV9-IGHMBP2 vector. The ubiquitously expressing *chicken-β-actin* (CBA) promoter is used to drive cDNA expression along with an optimized intron within the 5' leader sequence, as well as a synthetic polyA site (**Figure 1a**). To verify expression, HEK293 cells were transfected with the AAV9-IGHMBP2 plasmid, and western blot revealed the predicted IGHMBP2 product of ~110 kDa (**Supplementary Figure S1a**; **Supplementary Methods and Materials**). To validate the AAV9-IGHMBP2 expression in the CNS of *nmd* mice, 1×10^{11} viral particles were delivered via ICV at P3 and P6. Even though, this was not the optimized time-point for an ICV injection compared to P1 or P2, the initial goal was to authenticate expression of the AAV9-IGHMBP2 vector *in vivo*. AAV9-IGHMBP2 vector administration elevated IGHMBP2 protein levels in both brain and spinal cord compared to the untreated controls demonstrating that *in vivo* expression was readily detectable (**Supplementary Figure S1b,c**). To examine transgene expression at later stage, a relatively high dose (2×10^{11}) was injected into homozygous *nmd* mice at P2-3 which led to substantially increased IGHMBP2 levels in the spinal cord at 30 days postinjection (**Figure 1b**,**c**). We chose to deliver AAV9-IGHMBP2 directly to the CNS via an ICV injection. This type of delivery leads to robust AAV9 expression in the majority of the CNS tissues including a variety of neuronal populations and glia. Additionally, ICV injection at neonatal time points results in peripheral transduction due to the immature nature of the blood–brain barrier. We have previously shown that AAV9-GFP vector injected via ICV leads to robust GFP expression in peripheral organs (**Supplementary Figure S2**).[20]

Phenotypic assessments of vector-treated *nmd* mice

For the entire phenotypic analysis, *nmd* mice were treated with ICV injections of the AAV9-IGHMBP2 vector using two doses; a low dose (1.25×10^{11} vg, total of 12 µl) delivered at P2 and P3, and a high dose (2.5×10^{11} vg, total of 24 µl) delivered at P2, P3, and P4. The elevation in IGHMBP2 levels was confirmed by western blot in both low- and high-dose-injected SMARD1 compared to untreated SMARD1 10 days post last injection (**Figure 1d**). The increase in IGHMBP2 expression was directly correlated to the injected dose (**Figure 1e**).

The *nmd* mouse model resembles the milder form of the disease and 35% of the untreated animals in our colony survived 11 months to a year. To ensure the accuracy of the survival results, the untreated mice were not sacrificed when their strength was deteriorating due to the fact that they could still survive for months after a diminution in their activity level. Approximately 14% of untreated *nmd* mice died at P19-P22. We hypothesized that this fatality is likely due to a significant decrease in IGHMBP2 protein levels between postnatal days 10–21 as previously reported.[18] The fatality rate of low-dose-injected animals at this time period was negligible compared to untreated (6 versus 14%); and low-dose-treated *nmd* mice survived significantly longer than untreated ($P = 0.001$; 364 days median survival in low-dose-treated compared to 151 days in untreated) (**Figure 2a**). Surprisingly, the mortality rate at P19-22 for the high-dose-injected *nmd* mice increased to 30% and the survivors had a drastically shorter life span than untreated and low-dose treated ($P < 0.0001$) (**Figure 2a**). To rule out the possibility of multiple ICV injections as the cause of death, we treated several animals ($n = 7$) by a single IV injection using the high dose and yet 28% of the IV-injected animals died at predicted time point (**Supplementary Table S1**), suggesting that this mortality depends on the dose rather than the strain of multiple ICV injections. One unexpected turn in our survival analysis was that both virus and sham injection by ICV route led to development of hydrocephalus in both heterozygous and homozygous *nmd* mice within 1–1.5 months postinjection (**Supplementary Figure S3**). The frequency of hydrocephalus was 13% (2/15) in low-dose-treated *nmd* animals (**Figure 2a**), and 25% in sham-injected heterozygous and homozygous *nmd* (**Supplementary Table S1**). Surprisingly, the incidence of hydrocephalus was 40 to 41% in high-dose vector-treated heterozygous and homozygous *nmd*, respectively (**Supplementary Table S1**). Treated homozygous *nmd* animals which developed hydrocephalus appeared to be rescued phenotypically and had similar activity level as normally developed treated mice but were sacrificed at the predefined end-stage and excluded from further functional analysis. Hydrocephalus was specific to *nmd* genetic background since it never occurred in heterozygous SMA mice treated with ICV delivery of high-dose AAV9-IGHMBP2. On the contrary, it also occurred in homozygous and heterozygous *nmd* mice treated with ICV delivery of high-dose control virus, scAAV9-GFP (14 and 25%, respectively) (**Supplementary Table S1**).

To demonstrate the potential gender-based sensitivity to high dose, we graphed the survival curve of treated and untreated adult mice according to their gender (**Figure 2b**). This graph excludes all *nmd* mice that could not survive the initial side effects and did not reach adulthood. Our rational was that (i) the gender of mice dying early could not be determined due to immature growth of *nmd* mice, (ii) hydrocephalus was gender independent, and (iii) the main goal was to demonstrate the toxic effect of the high dose in adult mice. Most importantly, the majority of early side effects

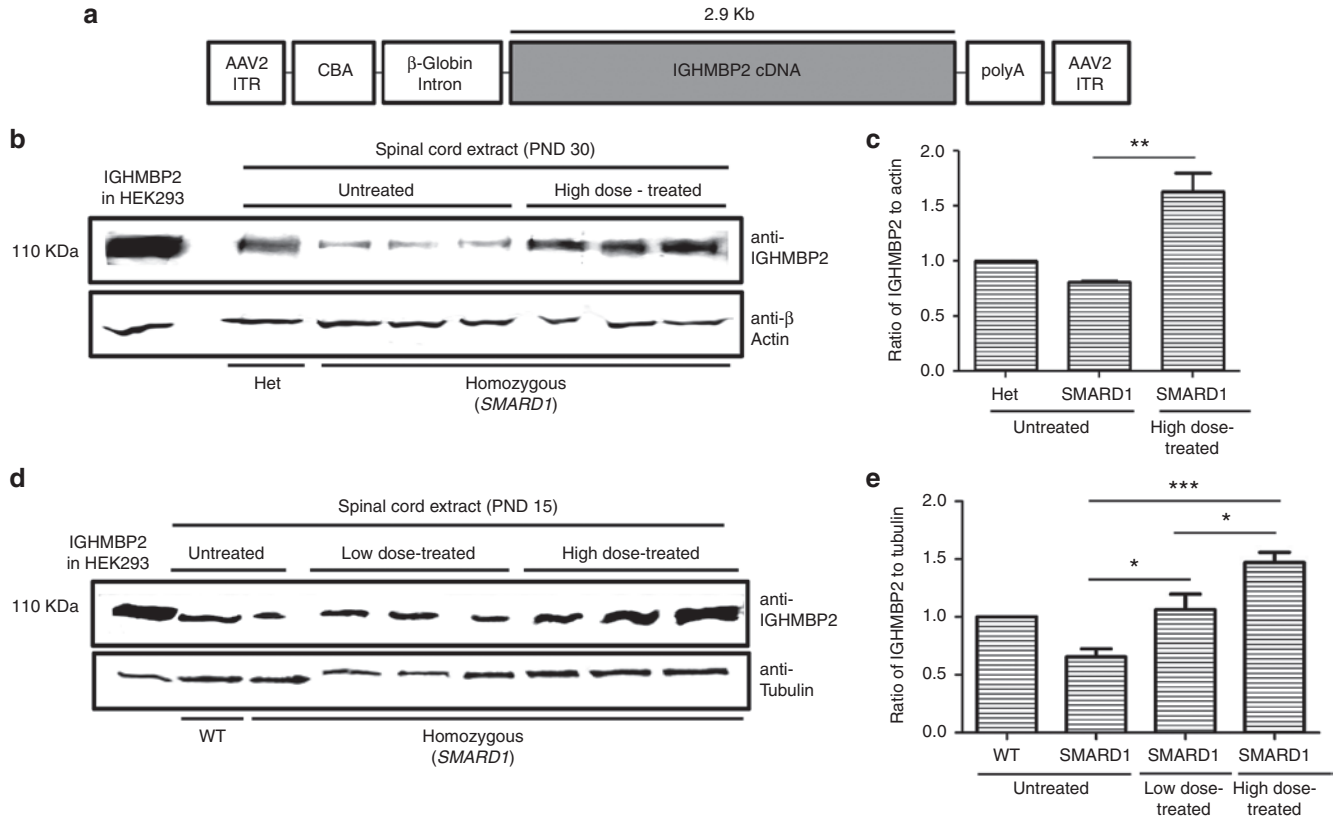

Figure 1 Development of a single-stranded adeno-associated virus (AAV) construct containing IGHMBP2 and expression of IGHMBP2 *in vivo*. (**a**) 2.9 kb of human IGHMBP2 cDNA under control of the ubiquitously expressing *chicken-β-actin* (CBA) promoter along with an optimized intron within the 5′ leader sequence and a synthetic polyA site were cloned into a single stranded AAV vector. (**b,c**) Western blot reveals increased levels of IGHMBP2 expression in spinal cord of homozygous *nmd* mice 30 days post-intracerebroventricular (ICV) injection of 2×10^{11} viral genomic copies. Tissue extracts of "Het" was used as positive control and anti-β-actin was used as loading control. (**d,e**) Western blot detects elevated IGHMBP2 expression in spinal cord extracts of low- and high-dose-treated SMARD1 mice 10 days post-ICV injection of 1.25×10^{11} (low-dose) and 2.5×10^{11} (high-dose) viral genomic copies. Tissue extract of WT was used as positive control and anti tubulin was used as loading control. HEK293 cells transfected with IGHMBP2 construct was utilized as size control in both gels. The expression level was normalized to IGHMBP2 levels in "Het" (**c**) and "WT" (**e**).

occurred in high-dose-treated animals and therefore, inclusion of mice with early complications would not change the final conclusion and establish even further that high dose is negatively affecting the SMARD1 mice. Both genders of the low-dose-treated *nmd* mice survived significantly longer than untreated and three out of four rescued males were capable of producing progeny suggesting a near-complete rescue. On the other hand, both genders of the high-dose-treated animals survived similarly to their untreated counterparts ($P = 0.21$, 120 days median survival in high-dose-treated males versus 151 days in untreated males; $P = 0.94$, 244 days median survival in high-dose-treated females versus 215 days in untreated females) (**Figure 2b**). While there was no significance in the survival of the high-dose-treated SMARD1 and their untreated counterparts, high-dose-treated females lived significantly longer than high-dose-treated males ($P = 0.01$) (**Figure 2b**) which could be potentially due to hormonal-based immune response. The high-dose-treated animals seemed completely rescued until their death which occurred either abruptly or in a short period of time. We conclude that ICV injection of low-dose AAV9-IGHMBP2 drastically extends the life span of both males and females, yet *nmd* mice are negatively impacted by high dosage of the therapeutic virus regardless of the delivery route, with males showing more sensitivity than females. In addition, ICV injections lead to hydrocephalus in *nmd* background and possibility of developing hydrocephalus is increased if accompanied by high dosage of the AAV9-IGHMBP2.

Consistent with the increased life span, AAV9-IGHMBP2 treatment in *nmd* mice significantly increased total body weight of both males and females compared to untreated littermates ($P < 0.0001$) (**Figure 2c**). The weight assessment (**Figure 2c**) includes all the animals treated with low and high dose. We also graphed the weight of low- and high-dose-treated SMARD1, which reached adulthood based on their gender to demonstrate a distinguishable weight difference between the genders (**Figure 2d**). Treated males gained more weight than treated females and this was in accordance with the fact that untreated males also weighed more than their female counterparts.

Functional tests include animals treated with both low and high dose and their activity level and strength were indistinguishable. Rotarod and grip strength tests were performed starting at P63 for 7 consecutive days/trials. Rotarod performance, as determined by the time an animal remained on the rotating cylinder, for treated males and females improved significantly compared to untreated counterparts ($P < 0.0001$) as AAV9-IGHMBP2-treated SMARD1 mice were indistinguishable from heterozygous ("Het") animals (**Figure 3a,b**). Treated SMARD1 animals (both genders) also demonstrated

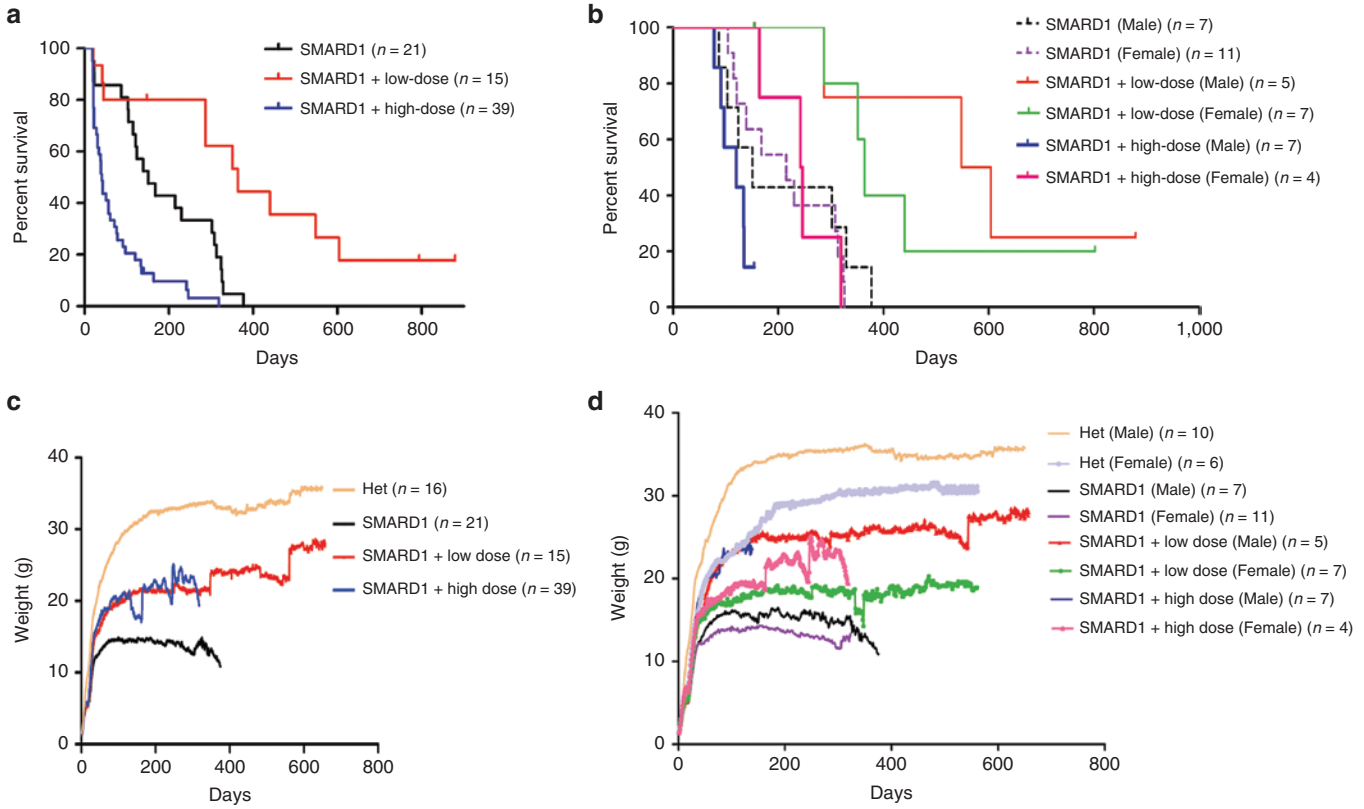

Figure 2 Intracerebroventricular (ICV) injection of AAV9-IGHMBP2 in low dose significantly increases the survival and total body weight in males and females *nmd*. (**a**) Homozygous *nmd* mice were injected ICV at P2 and P3 with 1.25×10^{11} and at P2, P3, and P4 with 2.5×10^{11} genomic copies of AAV9-IGHMBP2 and compared to untreated. Survival was determined by Kaplan-Meier curves and *P* value was determined by the log-rank (Mantel-Cox) test. Median survival of low-dose-injected *nmd* mice ($n = 15$) was 364 days compared to 151 days in untreated *nmd* ($n = 21$) ($P = 0.001$); median survival of high-dose-injected *nmd* ($n = 39$) was 41 days compared to 151 days in untreated ($P = 0.0001$) and 364 days in low-dose treated ($P < 0.0001$). (**b**) Survival of low- and high-dose-treated *nmd* based on their gender. The median survival of low-dose-injected *nmd* females ($n = 7$) was 364 days compared to 215 days in untreated female ($n = 11$) ($P = 0.002$); median survival of high-dose-treated *nmd* females ($n = 4$) was 244 days compared to 215 days in untreated females ($P = 0.94$). The median survival of low-dose-injected *nmd* males ($n = 5$) was 576 days compared to 151 days in untreated males ($n = 7$) ($P = 0.01$); median survival of high-dose-treated *nmd* males ($n = 7$) was 120 compared to 151 days in untreated males ($P = 0.21$) and 576 days in low-dose-treated males ($P = 0.006$). (**c**) Weight assessment of low- and high-dose-treated *nmd* compared to untreated and "Het". The weight of low-dose-treated *nmd* is 21.96±0.17 g and high-dose treated 19.46±0.27 g compared to 13.17±0.12 g in untreated (one-way ANOVA $P < 0.0001$). (**d**) Weight assessment of low- and high-dose-treated *nmd* based on their gender. The weight of low-dose-treated *nmd* females ($n = 7$) is 17.51±0.128 g and high-dose-treated females ($n = 4$) 19.16±0.26 compared to 12.57±0.136 g in untreated females ($n = 11$) (one-way ANOVA $P < 0.0001$). The weight of low-dose-treated *nmd* males ($n = 5$) is 24.25±0.18 and high-dose-treated males ($n = 7$) 18.29±0.57 g compared to 14.12±0.14 g in untreated males ($n = 7$) (one-way ANOVA $P < 0.0001$). Graphs "a" and "c" include all the untreated and treated animals and graphs "b" and "d" are based on gender differences and only represent males and females that reached adulthood excluding the mice that either died early or developed hydrocephalus.

a significant improvement in their forelimbs compared with untreated SMARD1 as measured by grip strength test ($P < 0.0001$) (**Figure 3c,d**). However, forelimb strength of treated SMARD1 was still considerably less than "Het" ($P < 0.0001$). We also tested the contracture in the hindlimb (another well-known feature of the *nmd* mice) of treated and compared to untreated SMARD1. Within the second week of age, untreated *nmd* mice demonstrate a characteristic inability to splay their legs when suspended from the tail.[18] This phenotypic trait was tested in untreated mice which show severe contracture (**Figure 3e,f**), while all of vector-treated *nmd* mice had a superior ability to splay their legs widely and pull themselves up (**Figure 3f**) consistent with the weight and rotarod performance. Free movements in the cage in addition to Catwalk test demonstrate rescued motor function and gait in AAV9-IGHMBP2 treated *nmd* (**Supplementary Videos S1, S2, S3**; **Supplementary Methods and Materials**).

AAV9-IGHMBP2 improves muscle pathology in hindlimbs and diaphragm

One of the rationales for increased hindlimb strength is the improved muscle phenotype. We analyzed Verhoeff-van Gieson-stained cross sections of quadriceps and gastrocnemius muscles in 8-week-old untreated SMARD1, low-dose-treated SMARD1, and untreated "Het". Pathological changes such as extensive muscle fiber atrophy (replacement of muscle tissue by adipose tissues), marked variability in muscle fiber size, centralized nuclei, and interstitial/periarterial fibrosis (collagen accumulation demonstrated by pink color in Verhoeff-van Gieson staining) were abundant in both types of muscles in untreated *nmd* (**Figure 4a,e**). These pathological features were rescued in the muscles of treated animals to a great extent (**Figure 4a,e**) as evidenced by an increase in the ratio of gastrocnemius weight to total body weight ($P < 0.0001$) (**Figure 4b**), a significant increase in the muscle fiber area ($P < 0.0001$)

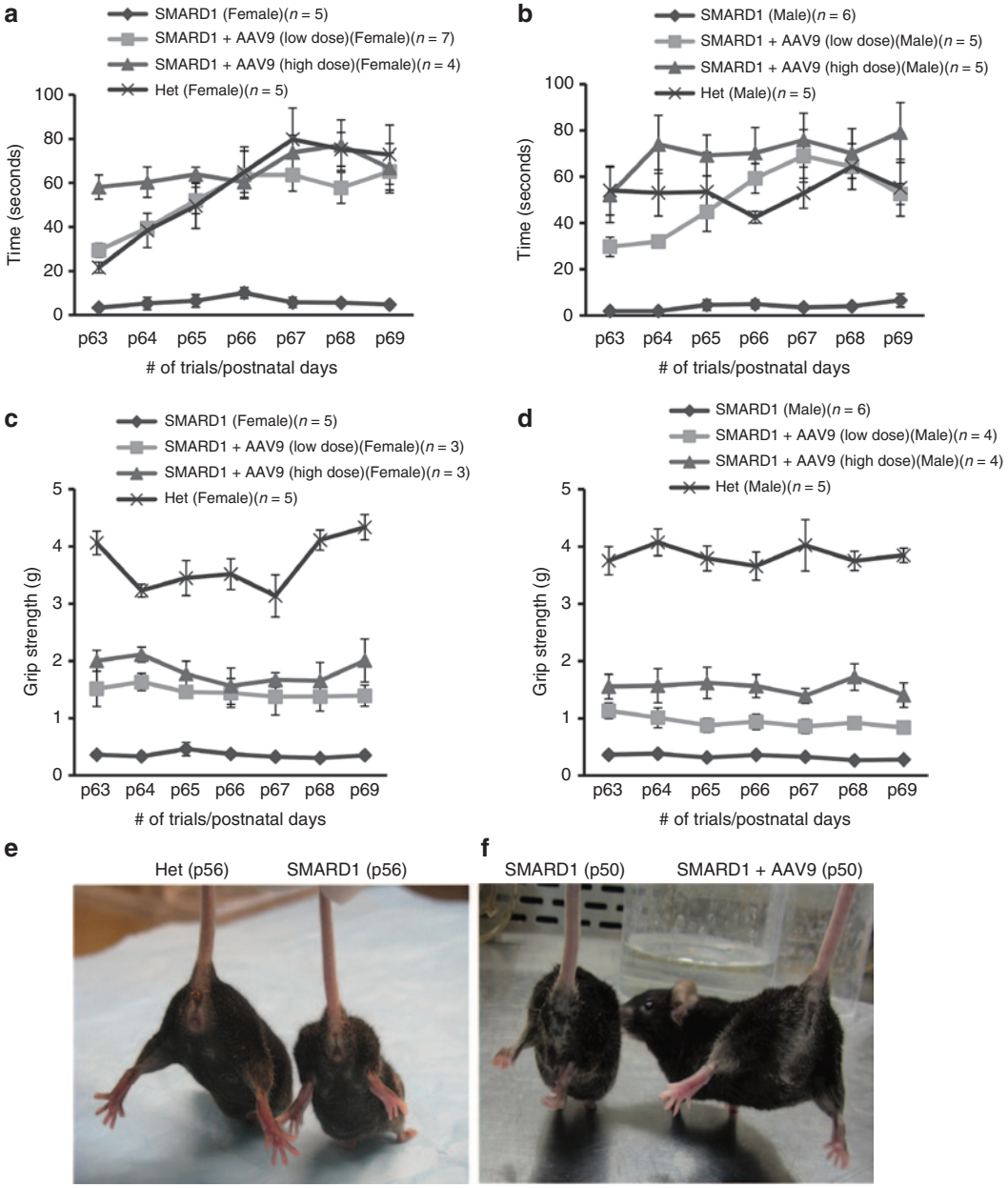

Figure 3 AAV9-IGHMBP2 strengthens the hindlimb and forearms of *nmd* females and males. (**a**,**b**) Rotarod performance was used to measure riding time parameter in seconds; low- and high-dose-injected *nmd* females (**a**) and males (**b**) were compared with the times of their age-matched untreated *nmd* littermates (one-way ANOVA $P < 0.0001$) and "Het" (one-way analysis of variance (ANOVA), ns). (**c**,**d**) Grip strength measurements in grams; low- and high-dose-treated *nmd* females (**c**) and males (**d**) were compared with their age-matched untreated *nmd* and "Het" littermates (one-way ANOVA $P < 0.0001$). Measurements were taken from P63 through P69. Error bars represent ± SE. (**e**,**f**) Suspended from the tail, all untreated *nmd* mice show severe hindlimb contracture compared with age-matched "Het" control (photo taken at P56) (**e**), while all AAV9-IGHMBP2-treated *nmd* have rescued hindlimb contracture compared to untreated (photo taken at P50) (**f**).

(Figure 4c,f) and a significant decrease in the intensity of fibrosis ($P < 0.0001$) (Figure 4d,g) compared to untreated. Diaphragmatic paralysis is one of the early features in SMARD1 patients but respiratory distress occurs in late stages of disease in *nmd* mice.[18] Verhoeff-van Gieson-stained cross and longitudinal sections of diaphragm muscles at 8 weeks of age (Figure 4h) revealed several pathological characteristics (centralized nuclei, muscle fiber atrophy, and fibrosis) in untreated but the diaphragm of treated SMARD1 mice mostly resembled that of "Het" animals with significant reduction in pathological features (Figure 4h–j). Our data suggest that AAV9-IGHMBP2 efficiently rescues the pathological alterations in the skeletal muscles.

AAV9-IGHMBP2 prevents loss of motor neurons in the ventral horn of lumbar spinal cord

As previously reported, the motor neuron numbers in the lumbar spinal cord of *nmd* mice are ~60% of the wild-type motor neurons at 10 days of age and motor neuron degeneration gradually continues until only 28% of motor neurons exist at 12–14 weeks of age compared to wild-type littermates.[18] To evaluate whether

AAV9-IGHMBP2 can prevent the loss of lumbar motor neurons, we quantified the total number of motor neurons in the ventral horn of L2 to L5 spinal cord in 8-week-old untreated SMARD1, low-dose-treated SMARD1, and untreated "Het" animals by Nissl staining and verified the results by ChAT immunostaining. The number of motor neurons in L2–L5 of untreated *nmd* animals was only 37% of the "Het" motor neurons ($P < 0.0001$) while this number increased to 59% in treated *nmd* mice when compared

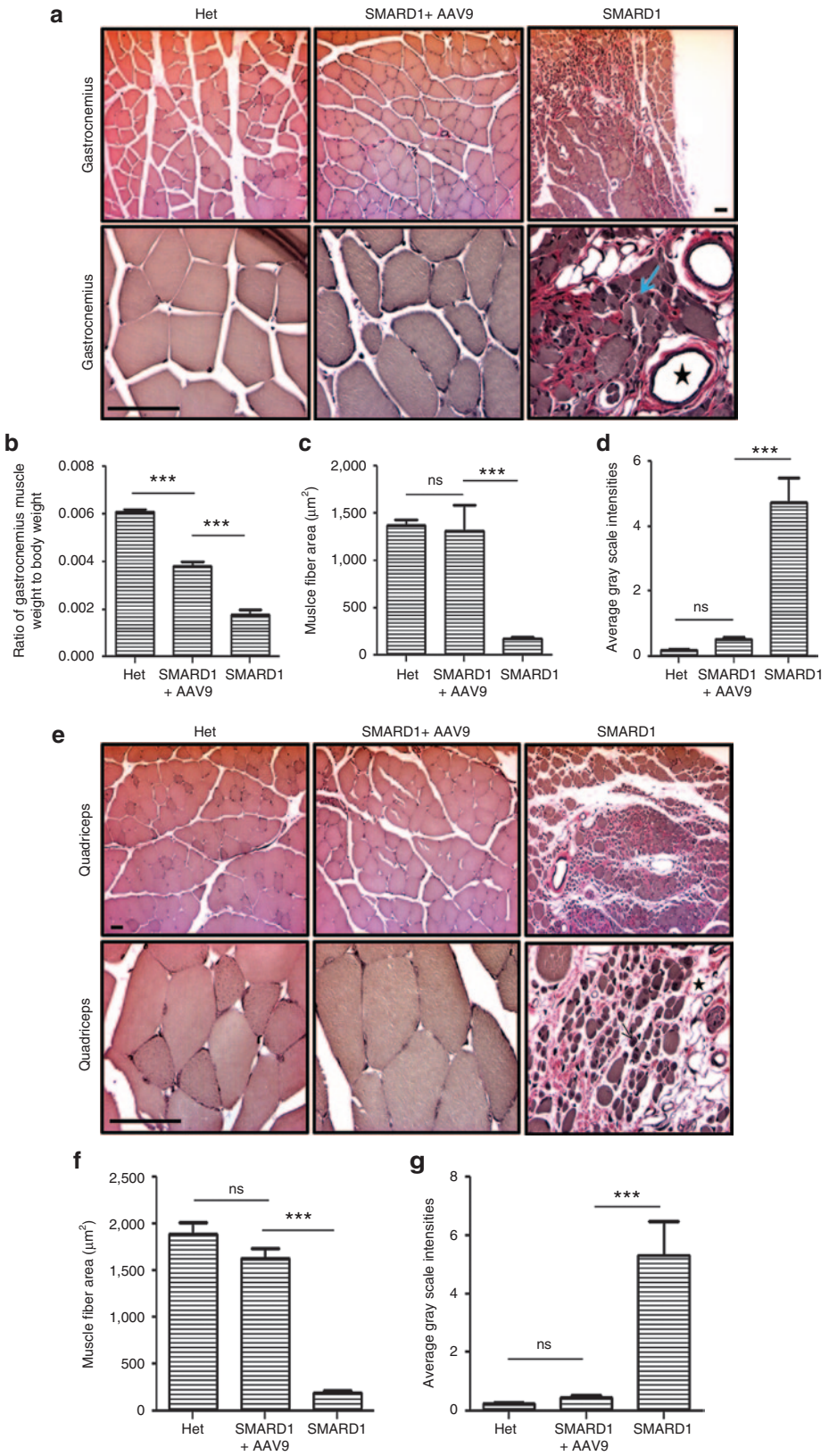

to "Het" animals (P = 0.007) (**Figure 5a**,**b**). The smaller size of motor neurons in untreated *nmd* compared to "Het" suggests hypertrophy which was also obvious in the treated *nmd* animals. Our results demonstrated that AAV9-IGHMBP2 injection led to increase in number of motor neurons compared to untreated (P = 0.003) even though this number is still significantly less than "Het".

AAV9-IGHMBP2 prevents denervation of gastrocnemius muscles

Muscle denervation in gastrocnemius and quadriceps of *nmd* mice initiates at 10 days of age and advances rapidly.[18] To determine whether AAV9-IGHMBP2 can mitigate the neuromuscular junction (NMJ) defects, we quantified the percentage of denervated, fully innervated and partially innervated motor endplates in teased fibers of gastrocnemius muscles at 8 weeks of age. Nearly all motor endplates of "Het" mice are fully innervated in contrast to untreated *nmd* mice which contain poorly developed NMJs with only 19% fully innervated motor endplates (P < 0.0001). Conversely, NMJs of treated *nmd* mice appear to be morphologically mature with ~59% fully innervated motor endplates (treated versus untreated P < 0.0001) (**Figure 5c**,**d**), which is consistent with increased motor neuron numbers in lumbar spinal cord. These results are evidence that AAV9-IGHMBP2 is capable of preventing another important pathological hallmark of SMARD1.

ICV injection of AAV9-IGHMBP2 prevents the loss of large diameter motor axons

Electrophysiological alterations in *nmd* mice have suggested axonal loss in sciatic and tibial nerves.[18] Additionally, *nmd* mice present with a significant loss of L4 motor axons, particularly in large diameter axons.[21] To determine whether AAV9-IGHMBP2 can rescue axonal defects, we quantified the number and diameter of all axons within the 5th lumbar motor root at 8 weeks of age (n of 4 for each group). As opposed to 4th lumbar root of which only a fraction of axons extends into the sciatic nerve, all of motor (ventral) and sensory (dorsal) axons of the 5th lumbar root expand into the sciatic nerve providing a pure population of axons in hindlimb. The images of the 5th motor root reveal several areas devoid of axons in untreated *nmd*, whereas motor root of treated *nmd* contains higher density of large diameter axons with fewer areas of axonal degeneration compared to untreated (**Figure 6a**). Total axon numbers were determined (**Figure 6b**) and the cross-sectional area of each axon was used to calculate the corresponding diameter. Distribution of axonal diameter in the motor root was displayed by grouping the axon diameters in 0.5 µm bins (**Figure 6c**). These data reveal that the total number of myelinated axons in untreated mice is only ~47% of that in "Het" animals, while treated mice contain ~64% motor axons compared to "Het" animals (P = 0.001) (**Figure 6b**). Importantly, radial axonal growth is improved in the motor root of treated *nmd* animals as indicated by significantly higher number of axons with maximal axonal diameter (ranging from 4.5 to 5.5 µm) compared to untreated (4.5–5 µm P = 0.007; 5–5.5 µm P = 0.02) (**Figure 6c**). These data provide direct evidence that AAV9-IGHMBP2 rescues axonal loss in 5th lumbar root.

AAV9-IGHMBP2 increases IGHMBP2 protein expression in lumbar motor *neurons*

The phenotypic correction of motor neurons, NMJ integrity, and axonal pathology likely occurs as a result of vector-mediated expression of IGHMBP2 in the appropriate target tissues, primarily lumbar motor neurons. To determine the percentage of transduction and the level of IGHMBP2 expression in the lumbar spinal cord, we performed double immunofluorescent staining using ChAT and IGHMBP2 antibodies in L2 and L5 spinal cord sections of untreated *nmd*, low-dose-treated *nmd*, and "Het" mice at 8 weeks of age. Quantification of IGHMBP2

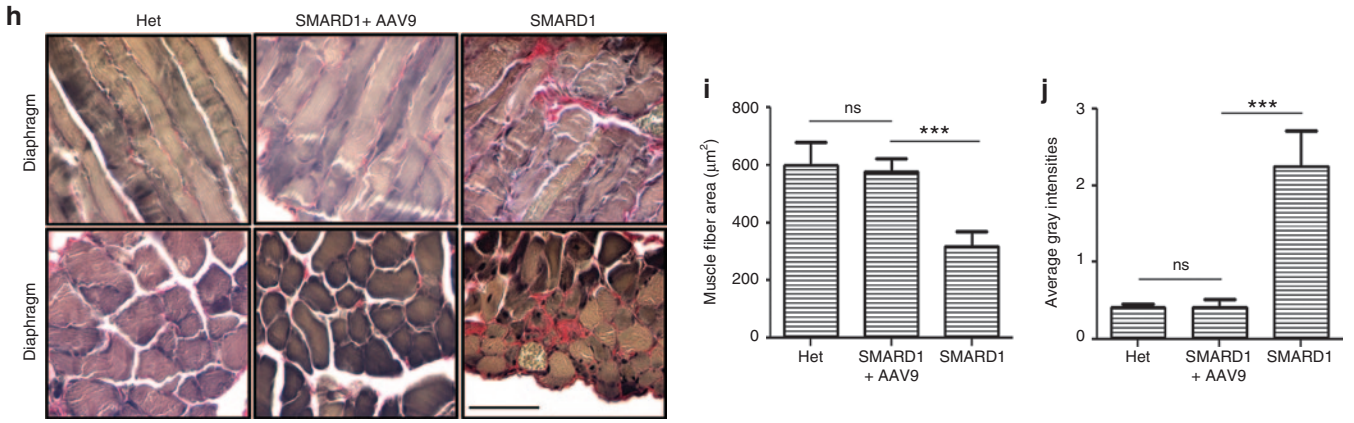

Figure 4 AAV9-IGHMBP2 repairs muscle pathology in gastrocnemius, quadriceps, and diaphragm. (**a**,**e**) Verhoeff-van Gieson-stained cross sections of gastrocnemius (**a**) and quadriceps (**e**) muscles of low-dose-treated males were examined at 8 weeks postinjection under 10× (top) and 40× (bottom) magnifications and compared with those of age-matched untreated *nmd* and "Het" (n = 4 for each group). (**h**) Verhoeff-van Gieson-stained longitudinal (top) and cross sections (bottom) of diaphragm of low-dose-treated males were examined at 8 weeks postinjection under 40× magnification and compared with those of age-matched untreated *nmd* and "Het" (n = 4 for each group). Untreated *nmd* mice demonstrate significant reduction in the muscle fiber area, replacement of muscles by adipose tissue (asterisks), centralized nuclei (arrow), and interstitial fibrosis (pink) while all of these defects have been significantly rescued in treated *nmd* mice (**a**,**e**,**h**). (**b**) The ratio of gastrocnemius weight to total body weight is increased in treated mice compared to untreated (one-way analysis of variance (ANOVA) P < 0.0001). (**c**,**f**,**i**) The area size of muscle fiber in treated *nmd* is significantly increased compared to untreated (one-way ANOVA P < 0.0001). (**d**,**g**,**j**) The intensity of interstitial/periarterial fibrosis is significantly decreased in the muscles of treated *nmd* compared to untreated (one-way ANOVA P < 0.0001). Scale bar = 200 m.

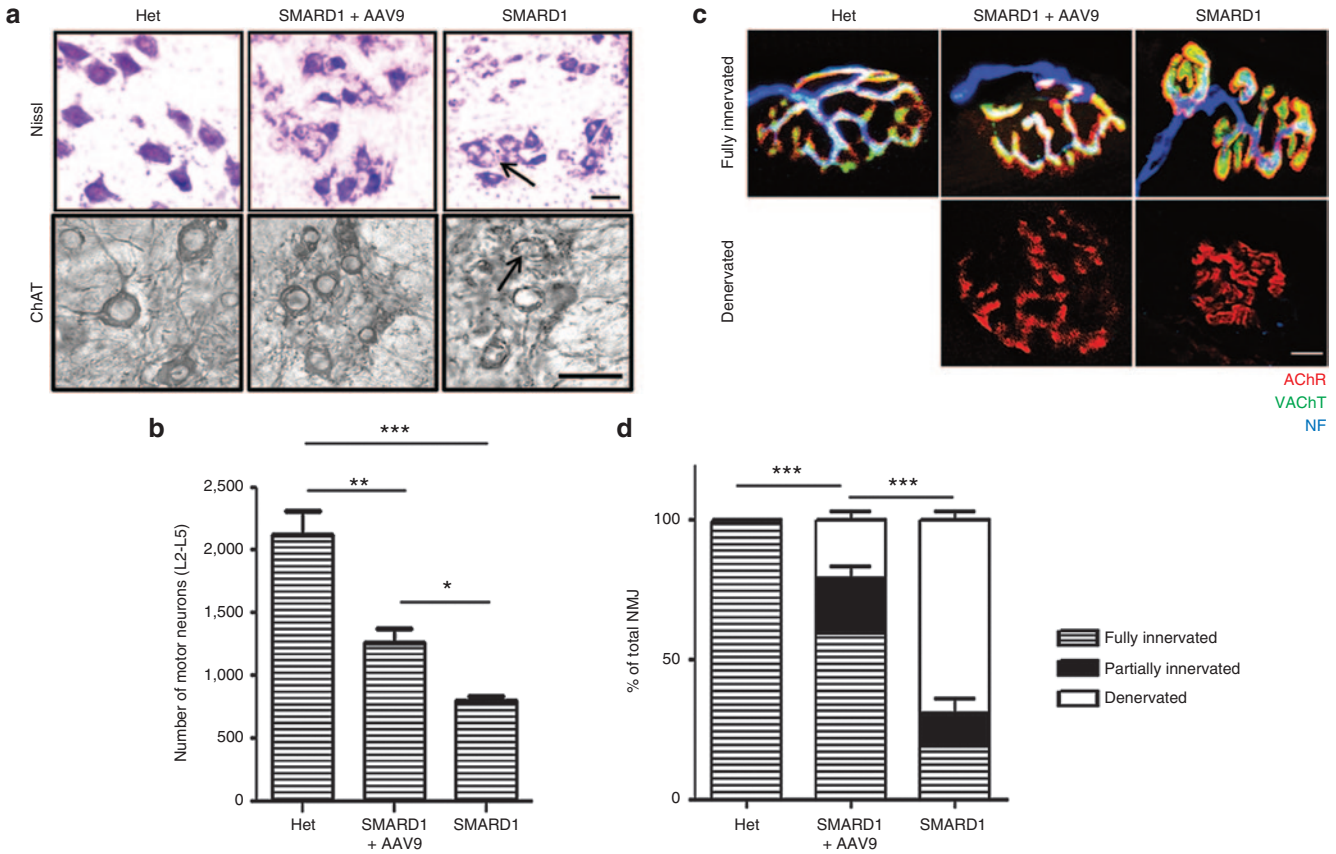

Figure 5 AAV9-IGHMBP2 rescues the loss in lumbar motor neurons and innervations of gastrocnemius. (**a**) Nissl-stained (top) and ChAT immunostained (bottom) cross sections of lumbar spinal cord in low-dose-treated males at 8 weeks of age compared to those of age matched untreated and "Het" littermates (n = 4 for each group), scale bar = 50 m. (**b**) Motor neuron counts in the ventral horn of lumbar spinal cord demonstrate a significant increase in total number of motor neurons in treated *nmd* compared to untreated (1261 ± 219 in treated versus 788 ± 96 in untreated, one-way analysis of variance (ANOVA) P = 0.003; 2,133 ± 368 in "Het" versus 1,261 ± 219 in treated, one-way ANOVA P = 0.007). Error bars represent mean ± SEM. Degenerated motor neurons are indicated by arrow and excluded in quantification. (**c**) NMJs from gastrocnemius muscle of low-dose-treated males at 8 weeks of age compared to those of age-matched untreated and "Het" littermates (n = 4 for each group). Muscles were labeled with α-BTX for AChRs, anti-neurofilament, and anti-vesicular acetylcholine transporter (VAChT) for nerve terminals, scale bar = 20 m. (**d**) Percentage of innervated, partially innervated, and denervated muscles; % of fully innervated in treated 59.285 ± 4.38 versus 19.54 ± 3.48 in untreated (one-way ANOVA P < 0.0001). Error bars represent mean ± SEM.

expression in ChAT-positive motor neurons by immunohistochemistry confirmed high levels of transduction in L2 and L5 spinal cord sections (84 and 58% compared to "Het", respectively) (three sections per region per animal; four animals in each group). The level of transduction correlated with the increase in the level of IGHMBP2 expression in ChAT-positive motor neurons of treated L2 (treated versus untreated P = 0.03) and L5 spinal cord (treated versus untreated P = 0.01) (**Figure 7a–d**). These results confirm the capability of AAV9-IGHMBP2 virus to reach and effectively transduce the target tissue resulting in increased IGHMBP2 levels in motor neurons.

DISCUSSION

SMARD1 possesses several important criteria that makes it particularly amenable to vector-mediated gene replacement, including: (i) it is a monogenic disease; (ii) the disease determining gene has been identified; (iii) an animal model exists that recapitulates many of the important hallmarks of the human condition; (iv) central nervous system tissues are fundamental to disease process and can be transduced with AAV9 vectors; and (v) there currently is no effective treatment for SMARD1. To build a solid foundation for advancement of SMARD1 gene therapy in preclinical studies, we have investigated key issues including the dosing effects, ICV delivery route, and the level of rescue by performing cellular analysis at 8 weeks of age and functional analysis at various time points. Our results using ICV delivery of a low titer of AAV-IGHMBP2 at P2 and P3 demonstrates the feasibility of the gene replacement therapy in rescuing the SMARD1 phenotype. The survival, weight gain, functional analysis and improvements of muscles, motor neuron numbers, motor axon numbers/diameter, and NMJ integrity confirm the ability of AAV9-IGHMBP2 to rescue the *nmd* mouse model at functional, cellular, and physiological levels. We also provide evidence that these improvements are the direct consequence of increased IGHMBP2 expression in the ChAT-positive lumbar motor neurons. However, ICV delivery of a higher dose (2.5×10^{11}) led to multiple adverse effects that negatively impacted the treated animals at various stages of development. One negative effect was higher incidence of early mortality at P19-22 (~30%) compared to low-dose (6%) and untreated (14%). The fatality rate during early time points was independent of the delivery route since it occurred with a similar

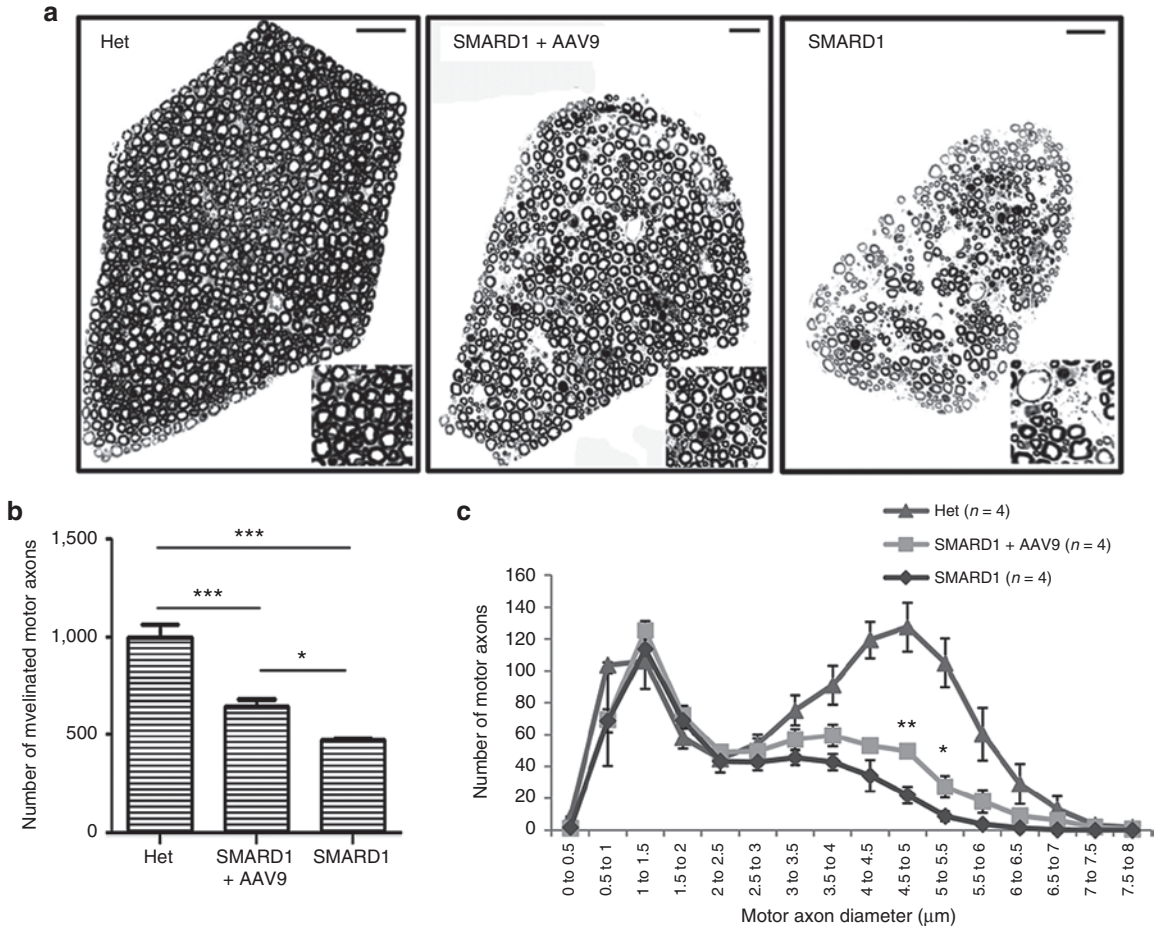

Figure 6 AAV9-IGHMBP2 increases the total number and diameter of motor axons in 5th lumbar ventral root. (**a**) Entire cross sections of 5th lumbar ventral root (magnified region on the corner) of low-dose-injected males at 8 weeks of age is compared to age-matched untreated and "Het" control ($n = 4$ animals per group) and shows a higher density of axons in treated compared to untreated *nmd* that contains many areas with axonal degeneration. Scale bar = 20 m. (**b**) Quantification of the total number of myelinated axons demonstrates a drastic increase in the treated *nmd* compared to untreated (648 ± 38.54 in treated versus 471 ± 6.18 in untreated, one-way analysis of variance (ANOVA) $P = 0.004$; 1,000.5 ± 62.32 in "Het" versus 648 ± 38.54 in treated, one-way ANOVA $P = 0.001$). (**c**) Distribution of axonal diameter for each treatment group at 8 weeks of age. Averaged distribution of axon diameters from the entire roots of four mice for each group demonstrates that peak axonal diameter (4.5–5 μm) is significantly increased in the treated animals compared to untreated (49 ± 4.36 in treated versus 22 ± 5.27 in untreated; one-way ANOVA $P = 0.007$). Error bars represent mean ± SEM.

incidence following IV delivery of the high dose, suggesting that it is dose dependent.

The high-dose-treated animals that evaded the critical stage of P19-P22 had a shortened life span compared to low-dose-treated animals, suggesting a potential toxic effect. Premature sudden deaths occurred after P100 in phenotypically rescued and seemingly healthy animals, potentially due to an impact upon the IGHMBP2's normal cellular functions, including immunoglobulin isotype switching. The fact that IGHMBP2 expression decreases to a great extent between P10-21 in wild-type *nmd* mice[18] suggests tightly controlled IGHMBP2 homeostasis. Therefore, overexpression of IGHMBP2 in many tissues/organs by AAV9 may result in more negative than beneficial outcomes. The level of susceptibility to high dosing was gender-dependent with males showing higher sensitivity than females. At present, it is unclear whether the toxicity was related to an immune-related function or one of IGHMBP2's less well-characterized activities.

Additional unexpected complication in our survival study was the incidence of hydrocephalus development within 1–1.5 months post-ICV injection. We concluded that hydrocephalus depends upon the *nmd* genetic background due to the fact that it never occurred in any of the ICV-treated SMA mice models using various viruses including AAV9-IGHMBP2, but it occurred even in sham injected and scAAV9-GFP-treated *nmd* mice (**Supplementary Table S1**). The incidence of hydrocephalus was higher in high-dose AAV9-IGHMBP2-injected *nmd* mice than low dose or sham/AAV9-GFP injected. This was not due to additional ICV injections or high volume of the injected materials, since sham- and AAV9-GFP-injected animals were treated with identical numbers of injections and volumes. Hydrocephalus mainly results from the lack of drainage of cerebrospinal fluid after a brain trauma leading to increased intracranial pressure and dilation of the ventricles. While multiple mechanisms are involved in development of hydrocephalus, one possibility is that astrogliosis and microgliosis which may result from brain trauma

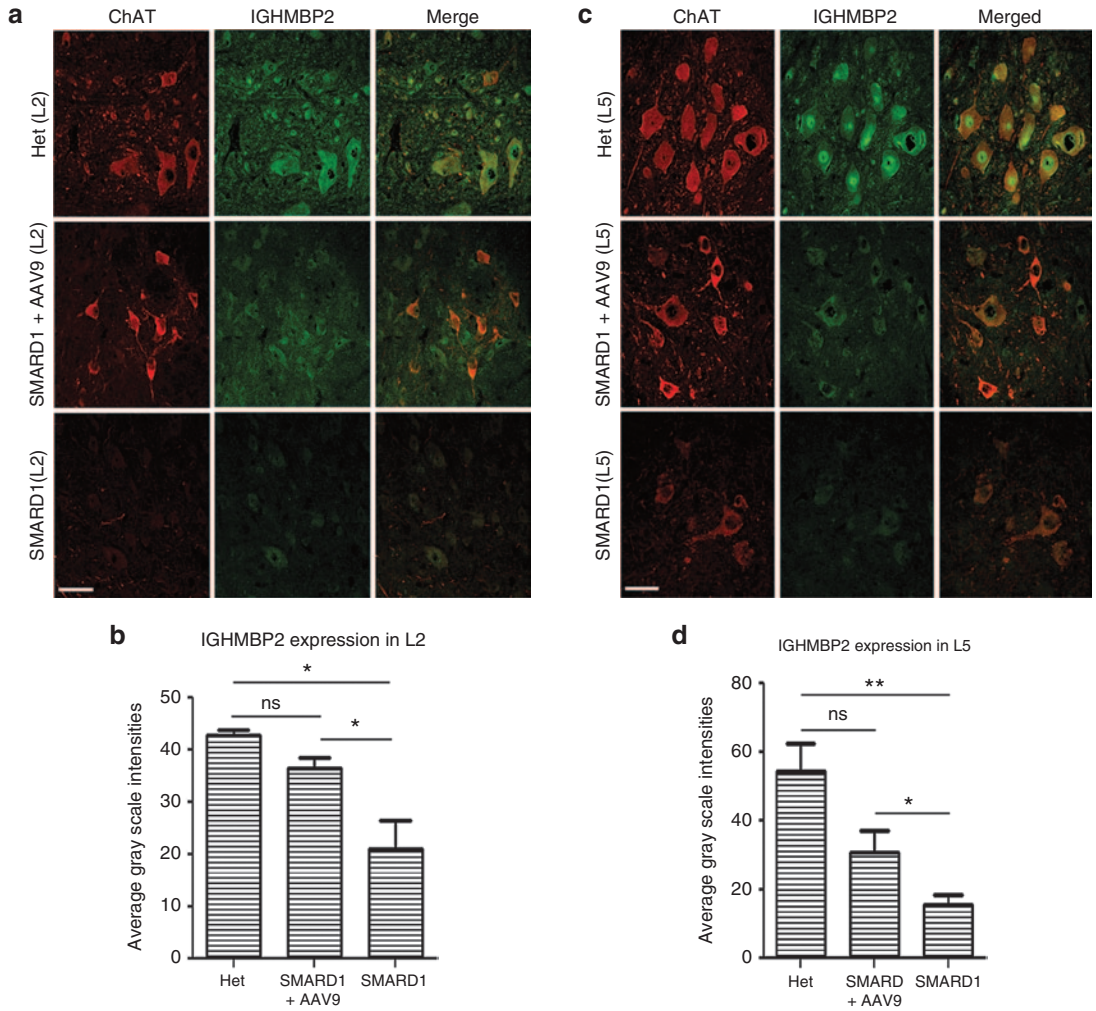

Figure 7 AAV9-IGHMBP2 treatment increases the level of IGHMBP2 expression in motor neurons of L2 and L5 sections of spinal cord. (**a,c**) Representative confocal fluorescent images of L2 (a) and L5 (c) spinal cord of low-dose-treated males at 8 weeks of age stained with ChAT (red) and IGHMBP2 (green) demonstrates the IGHMBP2 expression in ChAT-positive motor neurons and is compared to age-matched untreated and "Het" sections. The level of transduction is represented by gray scale intensities only in Chat-positive motor neurons relative to "Het". Scale bar = 50 µm. (**b,d**) Quantification of IGHMBP2 expression level in ChAT-positive motor neurons of treated males shows that IGHMBP2 levels is increased significantly in L2 (**b**) and L5 (**d**) compared to untreated (one-way analysis of variance treated versus untreated $P = 0.03$ in L2; $P = 0.01$ in L5). Error bars represent mean ± standard error of the mean.

are causing inflammatory response at the site of injury.[22] Our results heighten the importance of potentially damaging effects in *nmd* genetic background by ICV injection and AAV vectors, building the case for a thorough investigation in preclinical studies before advancement of a SMARD1 gene therapy toward clinical applications.

While preparing this manuscript, Nizzardo *et al.*[23] reported a gene replacement therapy with AAV9-IGHMBP2 using a single dose and a single delivery route (IV). Our survival results with high dose are in contrast with the survival results obtained by Nizzardo *et al.* in which 5×10^{11} viral genomic copies was delivered by IV injection and did not lead to early deaths or shortened life span. Interestingly, 70% of *nmd* mice treated with their empty AAV9 vector suffered early deaths at P20–25. Their report does not include the untreated animals and the baseline survival for their untreated is not known. The discrepancy in the survival data can be explained by differences in the delivery route and dosage of the virus, suggesting that a very high dose may be able to bypass the potentially detrimental side effects.

Currently, there are no effective treatments for SMARD1. While vector-mediated gene therapy is still in its infancy in terms of viable treatments, recent success in SMA has given hope that rare genetic diseases can become viable candidates for clinical trials. We have demonstrated the feasibility of a gene therapy strategy for SMARD1 but it is clear that gene replacement is not a one-size-fits-all strategy. Based on our data, the difference between an effective and a toxic dose via an ICV delivery is only twofold, suggesting a small therapeutic dose-range and emphasizing the importance of establishing precise levels of IGHMBP2 expression. Therefore, preclinical studies should focus on defining the therapeutic dose-range as well as the temporal window of AAV9-IGHMBP2 following ICV and IV delivery routes. In addition, the *nmd* genetic background seems more complex than SMA and hence, next steps should include a thorough investigation

of immune response to dose-escalation studies and toxicology studies in a second species such as pigs or nonhuman primates. While SMARD1 is a rare disorder, this type of research could provide evidence that a streamlined approach to gene replacement could fast-track translational therapies for rare disorders that are unlikely to attract large pharmaceutical companies any time soon. This would also provide a platform for other monogenic diseases and expand the portfolio of applications for gene therapy.

MATERIALS AND METHODS

Vector construction. IGHMBP2 cDNA was amplified from ORF expression clone for IGHMBP2 (GeneCopoeia) using IGHMBP2 forward (5′-aaacggccgtcggcttctaggggcccaggc-3′) and reverse (5′-gggaagcttggtcacgt cccctctccttc-3′) primers and cloned into *Eag I* and *Hind III* sites of the scAAV-SMN vector[24,25] to replace the SMN cDNA. Then, the resulting clone was used as the template to amplify the entire CBA promoter, β-Globin intron, IGHMBP2 cDNA, and the poly A using forward *Pme I* (5′–gggtttaaaccacgcgtggtacctctggtcgtta-3′) and reverse *Mlu I* (5′–aaacgcgtgaatagaatgacacctactcagac-3′) primers. The amplified fragment was cloned into the *Pme I* and *Mlu I* sites of the pMU2 plasmid containing AAV2 terminal repeats.[26] This final clone was developed into the single-stranded AAV9 virus using an appropriate packaging cell line. The virus expressing the full-length IGHMBP2 cDNA was purified by three CsCl density-gradient ultracentrifugation steps and dialyzed against HEPES buffer. Viral particles were titered by quantitative polymerase chain reaction using SYBR Green.

Transfection. The transfections were performed using 50 pmol/l of linear polyethylenimine per 1.0 µg of DNA as described previously.[27] The pMU2 clone containing IGHMBP2 cDNA was transfected into HEK293 cells grown to 80% confluence before transfection and cells were harvested 48 hours post-transfection. Controls include salmon sperm DNA equilibrated for total DNA transfection loads.

Animal procedures and injection. SMARD1 model mice (*nmd*) (B6.BKS-*Ighmbp2*$^{nmd\text{-}2J}$/J) were purchased commercially (Jackson Laboratories Bar Harbor, ME) and a colony was established. All animal experiments took place in accordance with procedures approved by NIH guidelines and MU Animal Care and Use Committee. SMARD1 animals were genotyped at P1 according to the genotyping procedure in Jax mice resources. *nmd* mice were ICV injected[25,28] with 1.25×10^{11} or 2.5×10^{11} viral genomes at p2 and p3 for low dose and an additional injection at p4 for higher dose. At 8 weeks of age, three groups of *nmd* mice (unaffected, treated, and untreated (*n* of 4 per each group)) were anesthetized with 2.5% isoflurane and then perfused transcardially with cold 0.1 M phosphate-buffered saline (PBS) (pH 7.4), followed by 4% paraformaldehyde in phosphate buffer (0.1 M, pH 7.4). The diaphragm was harvested before the perfusion and fixed in 4% paraformaldehyde overnight. The legs were incised following the perfusion and postfixed for additional 2 hours in 4% paraformaldehyde. The remaining body of the perfused mice was postfixed in 4% paraformaldehyde for 48 hours and the spinal cord and ventral roots were harvested.

Motor function tests. Motor activity and coordination were quantified using rotarod treadmill for mice (IITC Rotarod Series 8, IITC Life Science, CA) with the speed of 5 rotations per minute. The animals were placed on textured drums to avoid slipping. When the tested animal fell onto the individual sensing platform, the test results were recorded in seconds. For forelimb grip strength measurement, a grasping response test was utilized. Each pup's front paws were placed on a wire mesh (1-cm^2 grids) and gently dragged horizontally along the mesh (BioSeb Model BP32025, Vitrolles, FR, EU & Pinellas Park, FL). Any resistance felt was scored as a positive response. The strength of the animal holding onto the mesh before release was recorded in grams. Grip strength values (gram) were normalized against the animal's body weight. Both measurements were performed every day for 7 consecutive days starting on P63 and each value is the average of three trials performed on each day.

Western blot. Western blot with transfected HEK293 cells were conducted as described previously.[26,27] Blot was stripped with 30% H_2O_2/PBS (1:1) and reprobed with mouse antitubulin. Brain and spinal cord tissue harvested from treated animals were immediately placed in liquid nitrogen postharvest, and kept in −80 °C until protein extraction. Hundred micrograms of tissue were homogenized in 200–500 µl of Jurkat Lysis Buffer buffer and equal amounts of protein were loaded onto 10% sodium dodecyl sulfate polyacrylamide gel electrophoresis gel as previously described.[24,28,29] Blots were incubated overnight at 4 °C with rabbit IGHMBP2 antibody (Aviva Systems Biology, San Diego, CA) diluted to 1:1,000 and horseradish peroxidase anti-rabbit IgG (Jackson-Immunoresearch) was used as secondary antibody. Rabbit β-Actin and mouse Tubulin (Sigma, St. Louis, MO) was used as loading controls. Blots were visualized by chemiluminescence, images were captured by Fugi-Imager, LAS-3000, and quantified by Multi Gauge V3.0 software.

Muscle histology. 4-µm Verhoeff-van Gieson-stained cross-sections were prepared from quardriceps, gastrocnemius, and diaphragm muscles at the MU Veterinary Medical Diagnostic Laboratory. Muscle fiber area and interstitial/periarterial fibrosis were quantified using MetaVue as previously described.[24,30]

Nissl and ChAT immunostaining. L2–L5 spinal cord was dissected and immersed in 30% sucrose in 0.1 M PBS for at least 24 hours before OCT embedding. The 30-µm-thick cryosections were kept frozen in a solution containing glycerin, ethylene glycol, and sodium phosphate until the day of Nissl and immunostaining. For Nissl staining, sections were transferred to Super Frost positively charged slides and dried in slide warmer. Every fifth section (30-µm thick) from the L2–L5 was stained with 0.1% warm cresyl violet (Sigma) and mounted using Permount (Fischer Scientific) (total of 15 slides per animal). Images were captured using Leica DM 5500 B under 10× magnification. Nissl-stained α motor neurons in the anterior horns were determined according to the previously described morphological criteria,[31] where α motor neurons in the gray matter at the ventral horn were identified by their large size (cell body diameter >20 µm) and quantified by double blind counting. To confirm Nissl staining, ChAT immunostaining was performed with five sections (for each animal) selected from identical regions of L2–L5 which have been used for Nissl staining. Briefly, free-floating sections were washed three times with Tris-buffered saline and Triton-X100 (TBS containing 0.3 % Trition-X-100), incubated with 3% H2O2, blocked sequentially with Avidin (Dako North America, Carpinteria, CA), Biotin (Dako), and Protein block (Dako), each for 15 minutes. Then, sections were incubated with 1:300 dilution of Goat Anti-ChAT (EMD-Millipore, Temecula, CA) overnight. Biotynylated Link Universal Yellow (Dako) was applied followed by Streptavidin-Red (Dako), 30 minutes each. Finally, diaminobenzidine in Dako substrate was added and washed with distilled water as soon as the sections turned brown. The sections were mounted using Permount (Fischer Scientific), imaged using Leica DM 5500 B under 40× magnification. All ChAT-positive motor neurons located in the ventral horns of immunoreacted sections containing a nucleolus on the plane of the section were counted.

Neuromuscular junction immunostaining. Teased muscle fibers from gastrocnemius of 8 weeks age mice were labeled with α-BTX (Invitrogen) for AChRs, anti-neurofilament (Abcam), and antivesicular acetylcholine transporter (VAChT; synaptic system) antibodies for nerve terminals. Fluorescently labeled NMJs were observed with confocal microscopy and quantified as previously described.[32,33]

Ventral root processing and axon morphological analysis. Ventral root processing and axon analysis was performed as previously reported.[34] In brief, fifth lumbar nerve roots were dissected, treated with 2% osmium tetroxide, washed, dehydrated, and embedded in Epon-Spurr resin. Thick sections (2 µm) for light microscopy were stained with ρ-phenylenediamine. Images of cross sections of L5 motor axons were collected with a Zeiss Axio Imager A1 light microscope (Carl Zeiss MicroImaging GmbH, Jena, Germany). Cross sections of L5 motor were analyzed in at least four mice

per group. Entire roots were imaged, imaging thresholds were selected individually, and the cross-sectional area of each axon was calculated and reported as a diameter of a circle of equivalent area using the AxioVision Digital Image Processing Software (Carl Zeiss MicroImaging). Axonal diameters were grouped into 0.5 μm bins and total number of axons and axonal diameter in three groups were analyzed for statistical significance by GraphPad Prism software.

Motor neuron immunohistochemistry. Free-floating sections from L2 and L5 were washed three times with Tris-buffered saline and Triton-X100 (TBS containing 0.3% Trition-X-100), blocked with 10% normal donkey serum in Tris-buffered saline and Triton-X100 for 1 hour, and incubated with 1:300 dilution of Goat Anti-ChAT ((EMD-Millipore) and 1:200 dilution of Rabbit anti-SMUBP2 (Abcam) overnight. The next day, following 3× washing, 1:1,000 dilution of secondary antibodies (Alexa-Fluor 647 donkey anti-Goat IgG (H+L) and Alexa-fluor 555 donkey anti-rabbit IgG (H+L)) (Invitrogen) were applied for 4 hours. Sections were washed, transferred to super-frost positively charged slides, and mounted using mowiol 4–88 (Sigma). Images were captured using a bi-photon confocal microscope (Zeiss LSM, 510/MLO) in MU Cytology Core under the same computer settings for all sections in each experiment. Gray scale intensities in ChAT-positive motor neurons were measured by MetaVue and MetaMorph.

Statistical analysis. The statistical significance in comparing three experimental groups (unaffected, treated, and untreated) in all the experiments was calculated using one-way analysis of variance and Bonferroni multiple comparison *post hoc* test. Analyses were performed with GraphPad Prism software; error bars represent means ± standard error of the mean. Significance in survival was determined with log-ranked (Mantel-Cox) test. Percentages were calculated as values from "Het" or "WT" were standardized as 100%.

SUPPLEMENTARY MATERIAL

Figure S1. Western Blot detects CBA-driven expression of the IGHMBP2 cDNA in HEK293 cells and mice tissues.

Figure S2. ICV delivery of scAAV9-GFP at P2 results in the transduction of peripheral organs.

Figure S3. Development of hydrocephalus in high-dose injected homozygous nmd mice by ICV delivery.

Table S1. Percentage of hydrocephalus and early deaths is demonstrated in heterozygous and homozygous nmd and SMA mice following different treatments.

Video S1. In cage movements of two untreated and two AAV9-IGHMBP2 (low-dose) treated females at 10 months of age are recorded.

Video S2. Catwalk test demonstrates the gait and locomotion of low dose AAV9-IGHMBP2 treated nmd female at 11 months of age.

Video S3. Catwalk test demonstrates the gait and locomotion of untreated nmd female at 11 months of age.

ACKNOWLEDGMENTS

We would like to thank Marie-Therese Khairallah, Kyra Florea, and Madeline Simon for technical assistance. We also appreciate the services rendered by MU Molecular Cytology Core, Electron Microscopy Core, and Veterinary Medical Diagnostic Laboratory. This work is supported by a MU Research Board Grant (C.L.L.); MU College of Veterinary Medicine Faculty Research Grant (M.S.); the SMA Foundation (C.P.K.); NIH/NINDS grant R21NS093175 (C.L.L. and M.S.); NIH R25 GM064120 (P.W.S.); and Missouri Spinal Cord Injury Research Program (M.L.G.). The authors declare no competing financial interests.

REFERENCES

1. Grohmann, K, Varon, R, Stolz, P, Schuelke, M, Janetzki, C, Bertini, E *et al.* (2003). Infantile spinal muscular atrophy with respiratory distress type 1 (SMARD1). *Ann Neurol* **54**: 719–724.
2. Rudnik-Schöneborn, S, Stolz, P, Varon, R, Grohmann, K, Schächtele, M, Ketelsen, UP *et al.* (2004). Long-term observations of patients with infantile spinal muscular atrophy with respiratory distress type 1 (SMARD1). *Neuropediatrics* **35**: 174–182.
3. Grohmann, K, Wienker, TF, Saar, K, Rudnik-Schöneborn, S, Stoltenburg-Didinger, G, Rossi, R *et al.* (1999). Diaphragmatic spinal muscular atrophy with respiratory distress is heterogeneous, and one form Is linked to chromosome 11q13-q21. *Am J Hum Genet* **65**: 1459–1462.
4. Grohmann, K, Schuelke, M, Diers, A, Hoffmann, K, Lucke, B, Adams, C *et al.* (2001). Mutations in the gene encoding immunoglobulin mu-binding protein 2 cause spinal muscular atrophy with respiratory distress type 1. *Nat Genet* **29**: 75–77.
5. Diers, A, Kaczinski, M, Grohmann, K, Hübner, C and Stoltenburg-Didinger, G (2005). The ultrastructure of peripheral nerve, motor end-plate and skeletal muscle in patients suffering from spinal muscular atrophy with respiratory distress type 1 (SMARD1). *Acta Neuropathol* **110**: 289–297.
6. Kaindl, AM, Guenther, UP, Rudnik-Schöneborn, S, Varon, R, Zerres, K, Schuelke, M *et al.* (2008). Spinal muscular atrophy with respiratory distress type 1 (SMARD1). *J Child Neurol* **23**: 199–204.
7. Kaindl, AM, Guenther, UP, Rudnik-Schöneborn, S, Varon, R, Zerres, K, Gressens, P *et al.* (2008). [Distal spinal-muscular atrophy 1 (DSMA1 or SMARD1)]. *Arch Pediatr* **15**: 1568–1572.
8. Viollet, L, Barois, A, Rebeiz, JG, Rifai, Z, Burlet, P, Zarhrate, M *et al.* (2002). Mapping of autosomal recessive chronic distal spinal muscular atrophy to chromosome 11q13. *Ann Neurol* **51**: 585–592.
9. Fukita, Y, Mizuta, TR, Shirozu, M, Ozawa, K, Shimizu, A and Honjo, T (1993). The human S mu bp-2, a DNA-binding protein specific to the single-stranded guanine-rich sequence related to the immunoglobulin mu chain switch region. *J Biol Chem* **268**: 17463–17470.
10. Cox, GA, Mahaffey, CL and Frankel, WN (1998). Identification of the mouse neuromuscular degeneration gene and mapping of a second site suppressor allele. *Neuron* **21**: 1327–1337.
11. Molnar, GM, Crozat, A, Kraeft, SK, Dou, QP, Chen, LB and Pardee, AB (1997). Association of the mammalian helicase MAH with the pre-mRNA splicing complex. *Proc Natl Acad Sci USA* **94**: 7831–7836.
12. Chen, NN, Kerr, D, Chang, CF, Honjo, T and Khalili, K (1997). Evidence for regulation of transcription and replication of the human neurotropic virus JCV genome by the human S(mu)bp-2 protein in glial cells. *Gene* **185**: 55–62.
13. Miao, M, Chan, SL, Fletcher, GL and Hew, CL (2000). The rat ortholog of the presumptive flounder antifreeze enhancer-binding protein is a helicase domain-containing protein. *Eur J Biochem* **267**: 7237–7246.
14. Zhang, Q, Wang, YC and Montalvo, EA (1999). Smubp-2 represses the Epstein-Barr virus lytic switch promoter. *Virology* **255**: 160–170.
15. de Planell-Saguer, M, Schroeder, DG, Rodicio, MC, Cox, GA and Mourelatos, Z (2009). Biochemical and genetic evidence for a role of IGHMBP2 in the translational machinery. *Hum Mol Genet* **18**: 2115–2126.
16. Guenther, UP, Handoko, L, Laggerbauer, B, Jablonka, S, Chari, A, Alzheimer, M *et al.* (2009). IGHMBP2 is a ribosome-associated helicase inactive in the neuromuscular disorder distal SMA type 1 (DSMA1). *Hum Mol Genet* **18**: 1288–1300.
17. Cook, SA, Johnson, KR, Bronson, RT and Davisson, MT (1995). Neuromuscular degeneration (nmd): a mutation on mouse chromosome 19 that causes motor neuron degeneration. *Mamm Genome* **6**: 187–191.
18. Grohmann, K, Rossoll, W, Kobsar, I, Holtmann, B, Jablonka, S, Wessig, C *et al.* (2004). Characterization of Ighmbp2 in motor neurons and implications for the pathomechanism in a mouse model of human spinal muscular atrophy with respiratory distress type 1 (SMARD1). *Hum Mol Genet* **13**: 2031–2042.
19. Krieger, F, Elflein, N, Saenger, S, Wirthgen, E, Rak, K, Frantz, S *et al.* (2014). Polyethylene glycol-coupled IGF1 delays motor function defects in a mouse model of spinal muscular atrophy with respiratory distress type 1. *Brain* **137**(Pt 5): 1374–1393.
20. Shababi, M, Osman, E and Lorson, C. Gene therapy in spinal muscuar atrophy (SMA) models using intracerebroventricular injection into neonatal mice (2015). In: Bo X and Verhaagen J (eds.). *Gene Delivery and Therapy for Neurological Disorders*. Humana Press: New York. pp. 297–320.
21. Maddatu, TP, Garvey, SM, Schroeder, DG, Hampton, TG and Cox, GA (2004). Transgenic rescue of neurogenic atrophy in the nmd mouse reveals a role for Ighmbp2 in dilated cardiomyopathy. *Hum Mol Genet* **13**: 1105–1115.
22. Miller, JM and McAllister JP, 2nd (2007). Reduction of astrogliosis and microgliosis by cerebrospinal fluid shunting in experimental hydrocephalus. *Cerebrospinal Fluid Res* **45**.
23. Nizzardo, M, Simone, C, Rizzo, F, Salani, S, Dametti, S, Rinchetti, P *et al.* (2015). Gene therapy rescues disease phenotype in a spinal muscular atrophy with respiratory distress type 1 (SMARD1) mouse model. *Sci Adv* **1**: e1500078.
24. Shababi, M, Habibi, J, Ma, L, Glascock, JJ, Sowers, JR and Lorson, CL (2012). Partial restoration of cardio-vascular defects in a rescued severe model of spinal muscular atrophy. *J Mol Cell Cardiol* **52**: 1074–1082.
25. Glascock, JJ, Shababi, M, Wetz, MJ, Krogman, MM and Lorson, CL (2012). Direct central nervous system delivery provides enhanced protection following vector mediated gene replacement in a severe model of spinal muscular atrophy. *Biochem Biophys Res Commun* **417**: 376–381.
26. Baughan, T, Shababi, M, Coady, TH, Dickson, AM, Tullis, GE and Lorson, CL (2006). Stimulating full-length SMN2 expression by delivering bifunctional RNAs via a viral vector. *Mol Ther* **14**: 54–62.
27. Coady, TH, Shababi, M, Tullis, GE and Lorson, CL (2007). Restoration of SMN function: delivery of a trans-splicing RNA re-directs SMN2 pre-mRNA splicing. *Mol Ther* **15**: 1471–1478.
28. Shababi, M, Glascock, J and Lorson, CL (2011). Combination of SMN trans-splicing and a neurotrophic factor increases the life span and body mass in a severe model of spinal muscular atrophy. *Hum Gene Ther* **22**: 135–144.
29. Shababi, M and Lorson, CL (2012). Optimization of SMN trans-splicing through the analysis of SMN introns. *J Mol Neurosci* **46**: 459–469.
30. Shababi, M, Habibi, J, Yang, HT, Vale, SM, Sewell, WA and Lorson, CL (2010). Cardiac defects contribute to the pathology of spinal muscular atrophy models. *Hum Mol Genet* **19**: 4059–4071.
31. Lance-Jones, C (1982). Motoneuron cell death in the developing lumbar spinal cord of the mouse. *Brain Res* **256**: 473–479.
32. Ling, KK, Lin, MY, Zingg, B, Feng, Z and Ko, CP (2010). Synaptic defects in the spinal and neuromuscular circuitry in a mouse model of spinal muscular atrophy. *PLoS One* **5**: e15457.
33. Ling, KK, Gibbs, RM, Feng, Z and Ko, CP (2012). Severe neuromuscular denervation of clinically relevant muscles in a mouse model of spinal muscular atrophy. *Hum Mol Genet* **21**: 185–195.
34. Barry, DM, Stevenson, W, Bober, BG, Wiese, PJ, Dale, JM, Barry, GS *et al.* (2012). Expansion of neurofilament medium C terminus increases axonal diameter independent of increases in conduction velocity or myelin thickness. *J Neurosci* **32**: 6209–6219.